THE JOURNAL OF THE ACOUSTICAL SOCIETY OF KOREA Vol.27, No.3E 2008. 9. pp. 84-94

Enhanced Strain Imaging Using Quality Measure

Mok-Kun Jeong*, Sung-Jae Kwon**
Departments of *Electronics and **Communications Engineering, Daejin University
(Received June 2, 2008; revised July 21, 2008; accepted September 1, 2008)

Abstract

Displacement estimation is a crucial step in ultrasonic strain imaging. The displacement between a pre- and postcompression signal in the current data window is estimated by first shifting the postcompression signal by the displacement obtained in the previous data window to reduce their decorrelation and then determining the remaining part of the displacement through autocorrelation and conversion of phase difference into time delay. However, since strain image quality tends to vary with the amount of compression applied, we propose two new methods for enhancing strain image quality, i.e., displacement normalization and adaptive persistence. Both *in vitro* and *in vivo* experiments are carried out to acquire ultrasound data and produce strain images in real time under the application of quasistatic compression. The experimental results demonstrate that the methods are quite effective in improving strain image quality and thus can be applied to implementing an ultrasound elasticity imaging system that operates in real time.

Keywords: *Autocorrelation, Phase difference, Displacement, Displacement normalization, Adaptive persistence*

I. Introduction

Ultrasonic strain imaging refers to a technique for mapping the strain distribution of a medium of interest under mechanical compression using ultrasound interrogation. It may be used to diagnose cancer or tumor whose strain is different from the surrounding tissue especially when there is little or no difference in reflectivity between them. In ultrasonic strain imaging using quasistatic compression, displacements are estimated and differentiated to produce a strain image [1-6]. Although crosscorrelation or speckle pattern matching methods can be employed for the direct estimation of displacements, their computational burden is quite high due in part to additional interpolation.

Autocorrelation-based methods have also been employed when computing displacement due to static compression in stain imaging [1-4]. When autocorrelation methods are adopted, phase difference should be converted to time delay. Since interpolation is not necessary and correlation functions do not need to be calculated at multiple lags in these methods, they are suitable for use in ultrasonic imaging systems that need to operate in real time. However, the center frequency of the signal should be exactly known for the accurate estimation of displacement [5, 6]. This is not an easy task in view of the fact that ultrasound signals have a broad bandwidth and the center frequency tends to vary over the range of imaging depths due to speckle and attenuation characteristics. Worse yet, if the displacement between the pre- and postcompression signals is large, the phase estimation error becomes large due to an increase in the decorrrelation. Moreover, the quality of strain image may suffer when the amount of compression applied varies with time.

In this paper, the calculated phase difference between the pre- and postcompression signals from the demodulated complex baseband signal is approximated

Corresponding author: Sung-Jae Kwon (sjkwon@daejin.ac.kr)
Department of Communications Engineering, Pocheon, Gyeonggi 487-711, Korea

using a first-order Taylor series. Since the resulting expression for the phase difference involves a term for the center frequency, the center frequency variation can be corrected for using a method for estimating the instantaneous frequency at every imaging depth [4]. In order to cope with large error due to large displacement, the postcompression signal is shifted against the precompression one by the amount corresponding to the delay obtained in the previous data window [5-7]. Due to the reduction of both displacement and decorrelation, the estimation becomes accurate. Furthermore, strain image quality can be improved by displacement normalization and adaptive persistence, a preliminary feasibility study of which is undertaken in [8]. The displacement profile of each scanline is normalized by the value of the displacement at a maximum imaging depth. Adaptive persistence is applied to individual strain image frames to reduce noise. The improvement of strain image quality is verified through simulations and experiments.

II. Estimation of Displacement and Strain

In this paper, complex baseband signals are used to estimate the displacement between pre- and post-compression signals reflected from tissue. The displacement is modeled by using an allpass filter whose phase varies linearly with frequency. In this case, the linear phase delay is the same as the group delay. Also, both are identical to the time delay, τ. If an input, $x_1(t) = r(t)\cos(\omega_0 t + \phi(t))$, is applied to the filter, then the output, which is a delayed version of the input, is given by

$$x_2(t) = x_1(t-\tau) = r(t-\tau)\cos(\omega_0(t-\tau) + \phi(t-\tau)), \quad (1)$$

where $r(t)$ is the envelope, ω_0 is the radian center frequency, and $\phi(t)$ is the time-varying phase. Following demodulation, their complex baseband signals can be expressed as

$$x_{b1}(t) = r(t)e^{j\phi(t)}$$

$$x_{b2}(t) = r(t-\tau)e^{j(-\omega_0\tau + \phi(t-\tau))}. \quad (2)$$

The phase difference between the two signals in a finite interval can be written as

$$\Delta\Phi_0 = \arg < x_{b1}(n) \cdot x_{b2}^{*}(n) >= \omega_0\tau + \phi(t) - \phi(t-\tau), \quad (3)$$

where arg denotes the phase of the argument, $<\cdot>$, the inner product, and $*$, the complex conjugate. Expanding $\phi(t-\tau)$ in a first-order Taylor series yields

$$\phi(t-\tau) \approx \phi(t) - \tau\phi'(t). \quad (4)$$

Thus, equation (3) can be simplified as

$$\Delta\Phi_0 = \omega_0\tau + \phi'(t)\tau. \quad (5)$$

Solving the above equation for τ, we obtain

$$\tau = \frac{\Delta\Phi_0}{\omega_0 + \phi'(t)} = \frac{\Delta\Phi_0}{\omega_0 + \omega_B(t)}, \quad (6)$$

where $\phi'(t) = \omega_B(t)$ is the derivative of phase with respect to time, corresponding to the instantaneous frequency. Hence,

$$\phi'(t) = \omega_B(t) = \frac{\arg < x_{b1}(n) \cdot x_{b1}^{*}(n+T) >}{T}, \quad (7)$$

where T is the sampling period. This term is responsible for reducing errors associated with the center frequency shift with increasing imaging depth due to speckle and attenuation characteristics. If $\omega_0 >> \omega_B(t)$, then equation (6) can be further simplified so that the following approximation

$$\tau = \frac{\Delta\Phi_0}{\omega_0} \quad (8)$$

can be used [3, 5].

If the displacement between two signals to be compared is large, their decorrelation becomes large, resulting in large errors in estimating the phase di-

fference. To make the phase difference as small as possible, our method of displacement estimation proceeds by shifting the postcompression signal, $x_{b2}(t)$, by the amount corresponding to a previously estimated coarse displacement, δ, as in the following expression:

$$x_{b2}(t+\delta) = r(t-\tau+\delta)e^{j(-\omega_0\tau+\phi(t-\tau+\delta))}. \quad (9)$$

The above process is graphically depicted in Fig. 1. Note that the waveforms in Fig. 1 represent either in-phase or quadrature components. Considering the fact that for proper operation, $|\tau-\delta|$ should be maintained less than one half of the period of the signal of interest, this shifting operation leads us to obtain valid displacement estimates.

Taking the inner product of $x_{b1}(t)$ and $x_{b2}(t+\delta)$ over a finite data window and calculating the phase, we get

$$\Delta\Phi_\delta = \arg < x_{b1}(t)\cdot x_{b2}^*(t+\delta) >= \omega_0\tau + \phi(t) - \phi(t-\tau+\delta). \quad (10)$$

Approximating the above equation using a first-order Taylor series expansion gives

$$\Delta\Phi_\delta = \omega_0\tau + \phi'(t)(\tau-\delta). \quad (11)$$

Hence, τ can be expressed as

$$\tau = \frac{\Delta\Phi_\delta + \phi'(t)\delta}{\omega_0 + \phi'(t)}. \quad (12)$$

Using the relationship that a temporal shift of δ is equivalent to a phase rotation of $e^{j(-\omega_0\delta)}$ and expanding in a Taylor series, we can obtain the following relationship:

$$\Delta\Phi_{\delta\delta} = \arg\left|< x_{b1}(t)\cdot x_{b2}^*(t+\delta) > \cdot e^{j(-\omega_0\delta)}\right| \approx \omega_0(\tau-\delta) + \phi'(t)(\tau-\delta). \quad (13)$$

Consequently, we obtain

$$\tau - \delta = \frac{\Delta\Phi_{\delta\delta}}{\omega_0 + \phi'(t)}, \quad (14)$$

where τ can be correctly determined from $\Delta\Phi_{\omega}$ as long as the latter is within the range $[-\pi, \pi]$ so as to avoid aliasing.

To obtain satisfactory displacement estimates, it is essential that δ should be as close to τ as possible. Since the displacement estimation starts at a depth of zero, as one gets deeper into the axial direction, the displacements of the current and previous data windows tend to be nearly identical. In subsequent simulation and experiment studies, in order to obtain the current displacement estimate, τ, we have used the previously estimated version of displacement, τ, for δ.

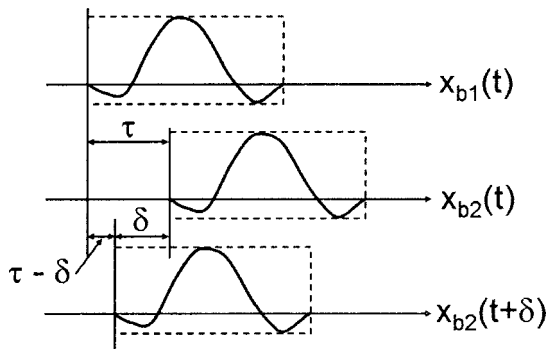

Fig. 1. (a) Reference, i.e., precompression signal, (b) postcompression signal, and (c) shifted version of (b) by the amount given by a previously estimated delay, δ.

III. New Methods for Improving Strain Image Quality

In quasistatic compression methods, the operator, who is usually an ultrasonographer, manually applies a sinusoidal compression with a transducer, so the amount of compression applied varies with time [9, 10]. Therefore, there is definitely a need to improve strain image quality and maintain it relatively constant [11, 12]. In order to accomplish this, we present two new methods in this paper.

One is the use of a quality measure in evaluating the quality of strain image. Using the quality measure, we normalize the displacement profile of every scanline in individual displacement images. More specifically, the normalization refers to dividing the displacement

profile, along the axial direction, of each scanline by the value of the displacement at a maximum imaging depth, so that we can obtain the same displacement at the maximum imaging depth across all scanlines. To eliminate low-quality strain images, Jiang et al. [9] proposed a performance descriptor that is given by the product of the correlation among motion-compensated radio frequency echo fields and the consistency among consecutive strain images. By contrast, our method focuses on reducing displacement variations from one scanline to another resulting from nonuniform stress distribution.

The other is the application of adaptive persistence processing to each frame to reduce strain image noise.

We have investigated the validity and efficacy of these new methods by simulations and experiments.

3.1. Normalization of displacement

The quality of strain image is proportional to the amount of applied compression over an intermediate range of strain [13]. Therefore, if the amount of compression applied can be determined, it can be used as a criterion for image quality.

The displacement at a maximum imaging depth tends to be proportional to the compression. We construct a graph, hereinafter to be termed maximum displacement curve (MDC), which plots the estimates of displacement at the maximum imaging depth across all scanlines. Although the MDC tends to fluctuate due to medium inhomogeneity and displacement misestimation, a parabolic curve fitting operation can produce a smoothly fitted maximum displacement curve (FMDC).

As a measure of the estimation error, we propose using the standard deviation, σ_{MDC}, of the fitting residuals between the MDC and FMDC as defined below:

$$\sigma_{MDC} = \sigma\{|MDC - FMDC|\}$$
$$\mu_{MDC} = \mu\{|FMDC|\}. \quad (15)$$

The standard deviation becomes large when there are displacement estimation errors due to the inhomogeneity and lateral motion in the medium. The average maximum displacement, μ_{MDC}, due to the applied compression can be found from the absolute value of the FMDC. MDCs are determined from displacement image based on experimental data, and then FMDCs are obtained, which can be classified into one of the following four cases:

(a) Case of μ_{MDC} being very small: Because the applied compression is small, the image quality is very poor.
(b) Case of FMDC having a zero-crossing: This corresponds to the case that there is a region whose displacement is identically zero.
(c) Case of FMDC being tilted: The applied compression differs from one scanline to the next, so the image quality differs depending on the scanline number. In this case, normalization improves the image quality significantly.
(d) Case of μ_{MDC} being very large: The image quality is already satisfactory, and thus no normalization is necessary.

The normalization serves the purpose of making the maximum displacement for each scanline the same by dividing the displacement profile of each scanline at each depth by the value of the FMDC at the maximum imaging depth. After normalization, the FMDCs at the maximum depth when connected together across all the scanlines will be nearly a straight line. In order to enhance the quality of strain image, it is recommended that strain image frames corresponding to the case of (a), in which μ_{MDC} is very small, and the case of (b), in which the FMDC has a zero-crossing, should not be displayed on the monitor.

3.2. Adaptive persistence

Because the quality of each frame of strain image is affected by the amount of applied compression, the image quality changes depending on, and thus is sensitive to, the operator's hand motion when a sequence of image frames is being displayed. This observation suggests that there is an advantage to employing adaptive persistence in the temporal domain to improve

the quality of each strain image frame. A persistence method used in conventional B-mode imaging merely averages consecutive image frames, degrading image quality when the constituent frames are of poor quality. In this paper, however, we introduce a quality metric, Q, which adaptively weigh between the present and past strain image frames to produce a high-quality output image, as in the following convex sum expression:

$$S_{out(n)} = Q \cdot S_{in(n)} + (1-Q) \cdot S_{out(n-1)}, \quad (16)$$

where $S_{in(n)}$ is the current input strain image frame, and $S_{out(n)}$ and $S_{out(n-1)}$ are the current and previous output strain image frames, respectively. Following this processing, the output strain image is displayed on the monitor. Depending on the value of Q, the adaptive persistence filter operates in one of the following three modes:

1) Case of Q: Because there is a significant amount of noise, the present frame is discarded, and the previous image frame is output again.
2) Case of $0<Q<1$: The weighted average of the present and past frames is output.
3) Case of $Q=1$: No persistence is used in this case, and only the present frame is output.

The quality metric, Q, used in equation (16), should be determined from strain images. We use two types of Q. One is an analytical quality (AQ) which can be considered objective since it can be calculated from an expression to be presented shortly, and the other is a subjective quality (SQ), which is a figure of merit determined by subjectively assessing the quality of each frame of strain images. The subjective grade is defined to take on an integer value from 0 to 4 with the corresponding strain image quality presented in Table 1.

μ_{MDC} is approximately proportional to the applied compression, and exhibits almost the same trend as SQ. Thus, the value of μ_{MDC} can be used as that of AQ, but those strain images with an SQ value of zero

Table 1. Grade and quality of strain image.

Grade	Quality of strain image
0	Poor
1	Outline visible
2	Inclusion discernible
3	Inclusion better discernible
4	Excellent

should be discarded completely. To this end, we define a parameter termed normalized standard deviation (NSD) as follows:

$$\sigma_{nMDC} = \frac{\sigma_{MDC}}{\mu_{MDC}^{n}}. \quad (17)$$

In order to find frames whose SQ value is equal to zero, we compute σ_{nMDC}. We set the power n to 3, and select a threshold for σ_{nMDC}. If the value of σ_{nMDC} is found to exceed the threshold, it is made to saturate. This is then followed by a normalization step to make the maximum value of σ_{nMDC} equal to unity. Because the values of σ_{nMDC} peak in most of the image frames whose SQ values are zero, we can remove those bad frames. In summary, we compute AQ from μ_{MDC} and σ_{nMDC} using the following expression:

$$AQ = \begin{cases} \mu_{MDC} / \max(\mu_{MDC}), \sigma_{nMDC} < Th, \\ 0, \quad \text{otherwise}, \end{cases} \quad (18)$$

where Th is a threshold that is determined empirically and $\max(\mu_{MDC})$ is the maximum value of μ_{MDC} over a certain number of consecutive strain image frames. The μ_{MDC} values can also be used as a quality measure. Thus, we remove bad frames whose SQ value is zero, and use μ_{MDC}, after normalizing it to unity, as a quality measure for the remaining frames. Because frames with a zero-crossing can be taken out by computing σ_{nMDC}, μ_{MDC} is not used in selecting those bad frames.

IV. Simulations

In order to verify equation (14), we generate ultra-

sound signals in a computer. By convolving random scatterers positioned along the axial direction with a 7.5 MHz center frequency and 60% bandwidth ultrasound pulse, we generate the received echo data consisting of 100 scanlines. To model the received signal after applying compression, the position of the random scatterers is changed depending on the amount of compression. The reflected echo corresponding to a precompression signal, $r(t)$, is obtained by convolving a transmit pulse, $p(t)$, and the impulse response, $s(t)$, of a distribution of random scatterers.

$$r(t) = p(t) * s(t), \tag{19}$$

where t is the temporal equivalent of depth. In order to produce a postcompression signal, $r_a(t)$, which is a strained version of $r(t)$, we transmit a temporally expanded version, $p(at)$, of the transmit pulse, $p(t)$, to a medium of interest, and obtain the following expression:

$$r_a(t) = p(t/a) * s(t), \tag{20}$$

where $a = 1/(1-\varepsilon) > 1$. Here, ε corresponds to the applied strain. If we temporally compress and attenuate $r_a(t)$, both by a factor of a, the rescaled output, $r_s(t)$, in terms of both amplitude and time can be written as:

$$r_s(t) = r_a(at)/a = p(t) * s(at). \tag{21}$$

Now the scatterers have a modified version of their original, uncompressed distribution, with the modification being a temporal compression by a factor of a. Then we estimate the displacement of $r_s(t)$ with respect to $r(t)$. To account for the center frequency downshift with increasing depth, an attenuation of 0.5 dB/cm/MHz is included by using a minimum-phase filter model [14].

Because we assume the elastic medium to be uniform, the displacement should increase linearly with increasing depth when compression is applied. Fig. 2 shows the displacement profile computed using equation (8) when a medium with an attenuation coefficient of 0.5 dB/cm/MHz is subjected to 0.1% compression. The vertical bars denote ± one standard deviation in displacement. With increasing imaging depth, the center frequency shifts downward and the displacement estimation error increases.

However, if we compensate for the center frequency shift using equation (14) and shift one signal against the other to reduce their decorrelation, we can reduce the displacement estimation errors as can be seen in Fig. 3. Even when the applied compression is large enough that the phase difference exceeds the angle range $[-\pi, \pi]$ at the maximum displacement, the resulting displacement is shown to be correctly estimated as can be seen in Fig. 4, where the estimation errors do not increase with depth. From Figs. 2 and 3, we can see that unless the center frequency shift due

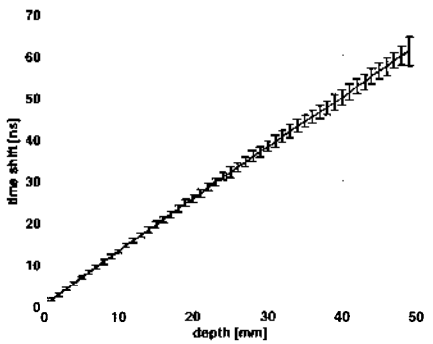

Fig. 2. Displacement estimated using equation (8) in a medium with an attenuation coefficient of 0.5 dB/cm/MHz when the applied compression is 0.1%. The vertical bars denote ± one standard deviation.

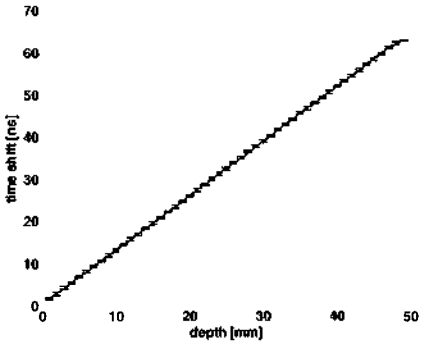

Fig. 3. Displacement estimated using equation (6) in a medium with an attenuation coefficient of 0.5 dB/cm/MHz when the applied compression is 0.1%. The vertical bars denote ± one standard deviation.

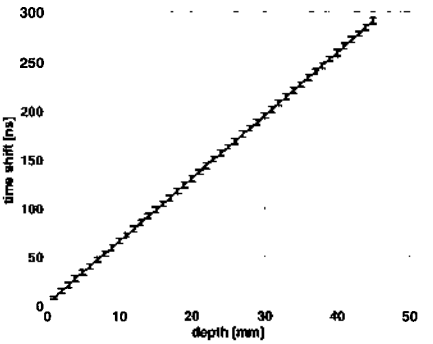

Fig. 4. Displacement estimated using equation (14) in a medium with an attenuation coefficient of 0.5 dB/cm/MHz when the applied compression is 0.5%. The vertical bars denote ± one standard deviation.

to attenuation is compensated for appropriately, the center frequency decreases with increasing depth and the displacements tend to be underestimated.

V. Experiments

Both *in vitro* and *in vivo* experiments were carried out to verify the proposed method. A manual cyclic compression was externally applied to an elasticity phantom (model 5864; CIRS, Norfolk, VA, USA) and a human subject using a 7.5 MHz linear transducer array. The baseband in-phase and quadrature data were acquired in real time from a clinical ultrasound scanner (Accuvix XQ; Medison, Seoul), and were transferred to a PC for signal processing. In all cases equation (14) was used to obtain results. Displacements were estimated by performing autocorrelation with a window length of 1 mm. The window length was empirically determined considering the estimation accuracy, center frequency, transducer bandwidth, and amount of compression applied. Successive data windows overlapped 50% of the window length.

The displacement and strain in the axial direction are estimated, and their corresponding images are presented in the left and right panels of Fig. 5, respectively. The strain image is obtained by differentiating the displacement profile along the axial direction. Both images are postprocessed by a 3-by-3 pixel median as well as boxcar averaging filter. The black circle represents a cylinder that is three times harder than the background. The cylinder has a diameter of 10 mm and is located at a depth of 30 mm.

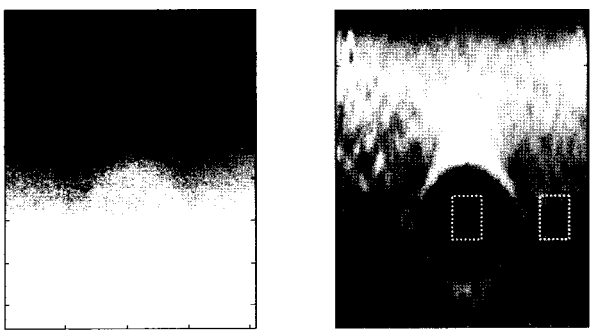

Fig. 5. Displacement (left) and strain (right) images.

In order to judge the quality of a strain image of interest, we use both elastographic contrast-to-noise ratio, CNR_e, and elastographic signal-to-noise ratio, SNR_e [15, 16]:

$$CNR_e = \frac{2(\mu_c - \mu_b)^2}{\sigma_c^2 + \sigma_b^2},$$

$$SNR_e = \frac{\mu}{\sigma}, \tag{22}$$

where μ_c and μ_b are the mean strain in the cylinder and background, respectively, σ_c and σ_b are the standard deviation of strain in the cylinder and background, respectively, and σ and μ are the standard deviation and mean of the entire strain image, respectively.

For the strain image shown in the right panel of Fig. 5, it is found that $\mu_{MDC} = 0.5422$, $\sigma_{MDC} = 0.0197$, $CNR_e = 40.8$ dB, and $SNR_e = 23$ dB. The dotted rectangular boxes in the figure indicate the areas used to compute CNR_e. When the center frequency is compensated for its variation, both CNR_e and SNR_e increase by about 0.3 dB. Because image processing is done in the figure, the effect of compensation is not very noticeable.

Fig. 6 depicts the MDC in solid line and the FMDC in dashed line for the displacement image in the left panel of Fig. 5. The results of parabolic curve fitting show that most of the MDCs can be smoothly fitted despite their fluctuations, implying that the compre-

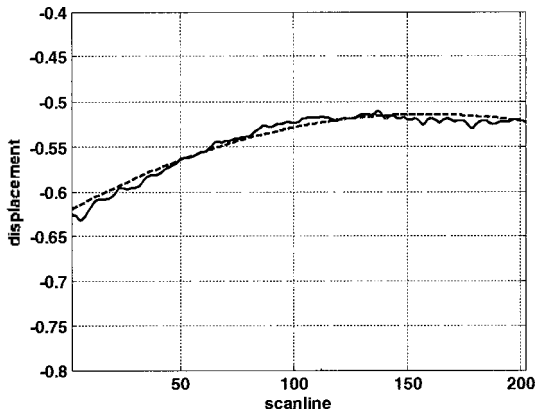

Fig. 6. Comparison of the MDC (solid line) and its FMDC (dashed line) obtained from Fig. 5.

ssion applied has propagated through the medium spherically [17]. We compare MDCs determined from experimental data and their corresponding FMDCs in Fig. 7, where the latter can be categorized into one of the four cases as mentioned in Subsection 3.1.

In Fig. 8, for each of the above four cases, the first and second columns are displacement images before and after normalization, respectively, and the third and last columns are strain images before and after normalization by the FMDCs in Fig. 7. In the cases of (c) and (d), there is an improvement in image quality, whereas there is no improvement in the cases of (a)

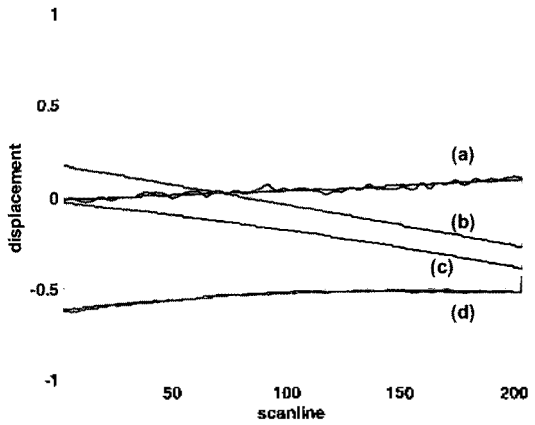

Fig. 7. Comparison of MDC and FMDC in four cases: (a) FMDC has small values, (b) FMDC has a zero-crossing, (c) FMDC is tilted, and (d) FMDC has large values.

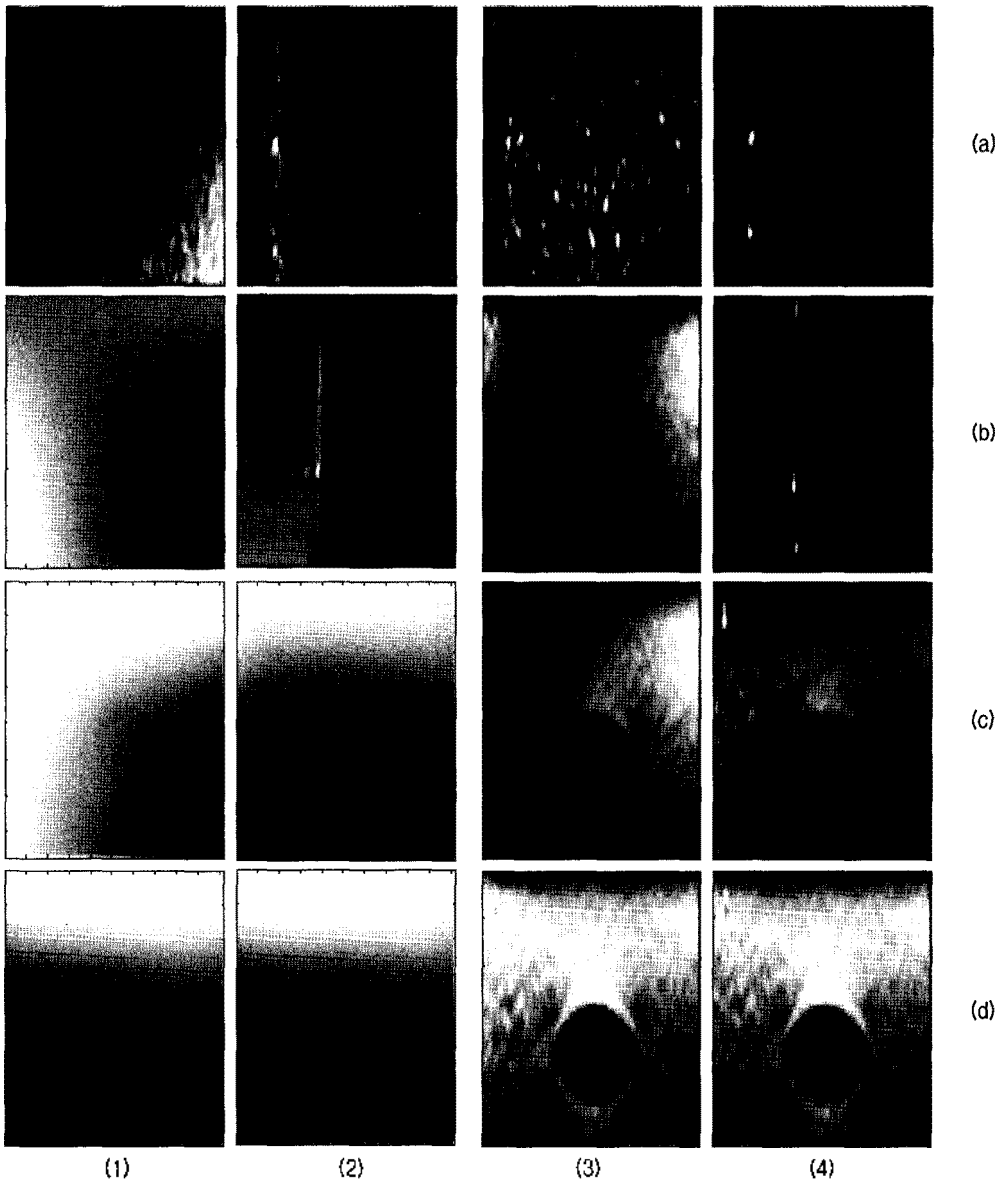

Fig. 8. For four cases of FMDCs labeled (a), (b), (c), and (d), columns 1 and 2 represent displacement images before and after normalization, respectively, and columns 3 and 4 represent strain images before and after normalization, respectively.

and (b). Fig. 9 shows what five grades of strain images each look like. Table 2 presents the values of μ_{MDC}, σ_{MDC}, CNR_e, and SNR_e for five grades of strain images shown in Fig. 9.

Fig. 10 compares the SQ and μ_{MDC}, where we can observe that there is good correlation between them. The number of evaluated consecutive strain image frames is 64. Fig. 11 shows that low-quality frames can be removed by utilizing the fact that σ_{nMDC} peak in most of the frames whose SQ values are zero. Fig. 12 compares the AQ and SQ as a function of the image frame number. We can see that the AQ computed from μ_{MDC} and σ_{nMDC} gives similar results as the SQ.

Table 2. Evaluation of parameters for each grade shown in Fig. 9.

Grade	μ_{MDC}	σ_{MDC}	CNR_e	SNR_e
0	0.033	0.0123	12.12	6.79
1	0.174	0.0075	11.49	10.85
2	0.699	0.0259	21.52	16.26
3	1.120	0.0395	35.74	21.60
4	0.542	0.0197	40.83	22.99

We compare plots of CNR_e and SNR_e versus the frame number in Figs. 13 and 14, respectively, after persistence processing based on the AQ values computed according to equation (18). The dotted lines indicate no persistence processing, and the solid lines represent the result of persistence processing, where small values of CNR_e and SNR_e are removed but large values are retained.

Fig. 15 compares the SQ and AQ values determined from *in vivo* human data. The dotted line denotes SQ values for 64 frames of a strain image sequence using the same method as used in the above phantom study, and the solid line indicates AQ values obtained by using $n=1$ in the denominator of equation (17). Because the solid and dotted lines exhibit a similar tendency, it can be seen that strain image quality can be assessed by using both μ_{MDC} and σ_{nMDC}. σ_{nMDC} is found to be small in the phantom where scatterers are uniform, but large in the human tissue which is inhomogeneous. Using a smaller value of n when calculating σ_{nMDC} is more effective in searching for bad frames.

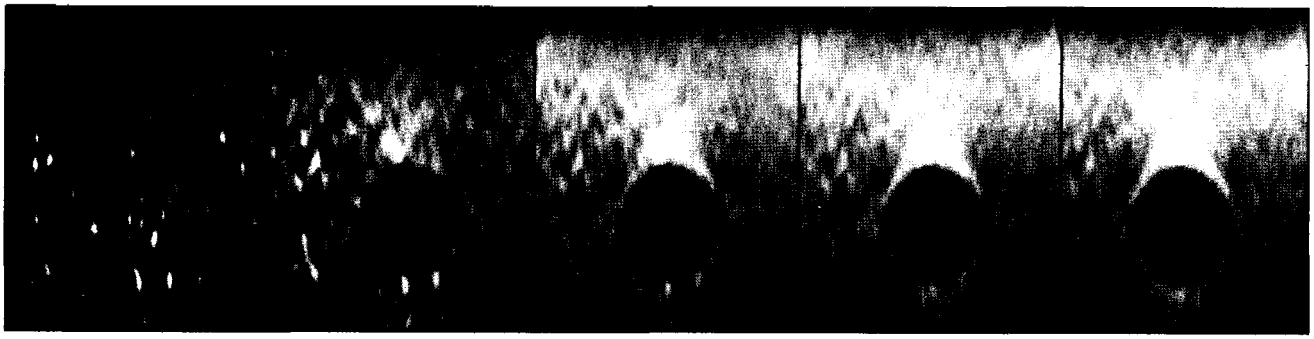

Fig. 9. Strain images and their quality grade.

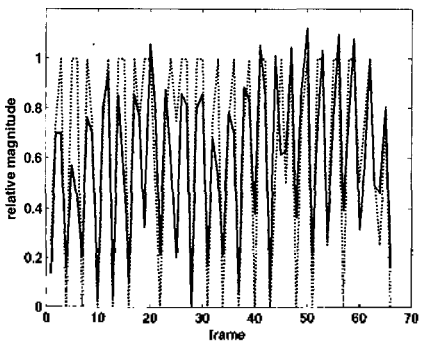

Fig. 10. Comparison of μ_{MDC} (solid line) and SQ (dotted line).

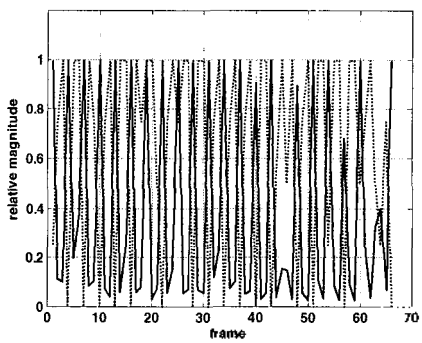

Fig. 11. Comparison of NSD (solid line) and SQ (dotted line).

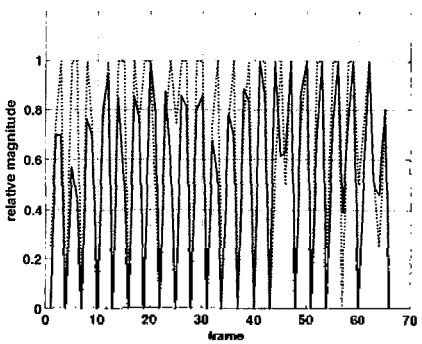

Fig. 12. Comparison of AQ (solid line) and SQ (dotted line) in phantom.

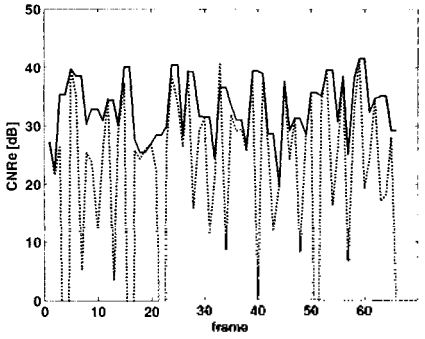

Fig. 13. Comparison of CNRe before (dotted line) and after (solid line) processing.

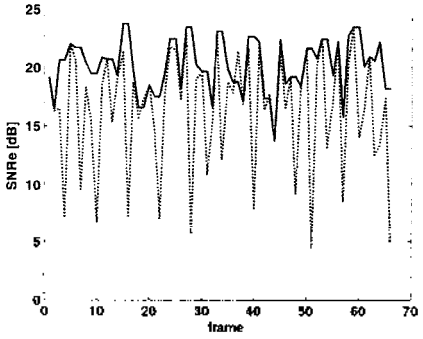

Fig. 14. Comparison of SNRe before (dotted line) and after (solid line) processing.

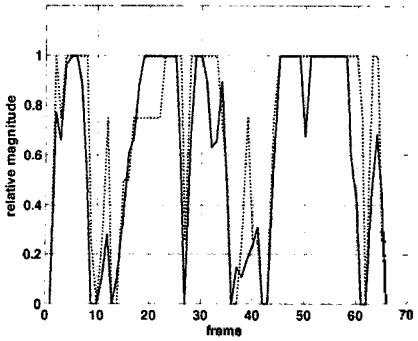

Fig. 15. Comparison of SQ (dotted line) and AQ (solid line) for a human volunteer.

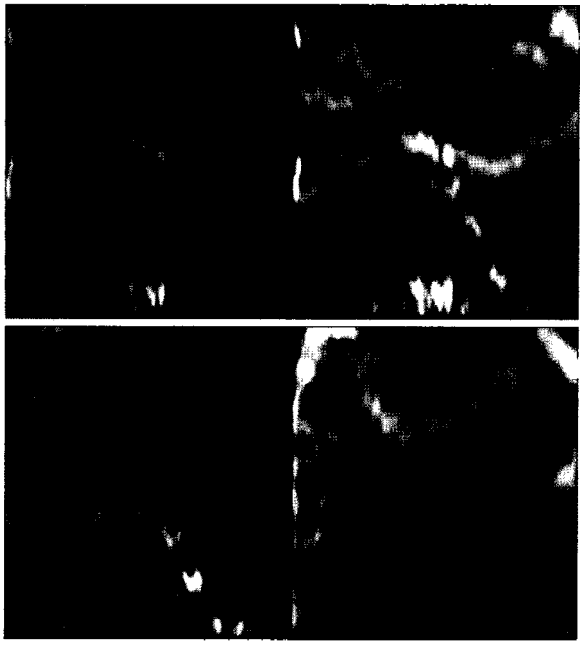

Fig. 16. Strain images before (left) and after (right) applying adaptive persistence processing where (a) and (b) correspond to frames 47 and 14 of Fig. 15, respectively.

The left and right panels of Fig. 16 correspond to strain images obtained by using AQ before and after persistence processing, respectively. Fig. 16(a) corresponds to frame 47 of Fig. 15, and shows a higher contrast following persistence processing. In Fig. 16(b) corresponding to frame 14 of Fig. 15, the unprocessed left image is of poor quality, while the right image shows improved quality after persistence processing.

VI. Conclusions

In order to produce strain images in real time on an ultrasonic scanner, displacements are estimated using the shift-compensated autocorrelation. We compensate for center frequency variation, and convert phase difference into time delay after shifting one signal relative to the other by the amount obtained in the previous data window. This method as well as new quality measures is applied to real-time elasticity imaging to obtain strain images of a phantom and a human volunteer with the result that the estimation error is relatively small. Both MDC and FMDC are obtained to evaluate the quality of strain images, and are confirmed to be directly related to image quality. The problem that strain image quality changes with time while applying a quasistatic compression using a transducer array is mitigated by employing newly proposed quality measures.

Acknowledgments

The authors would like to thank the anonymous reviewers for their efforts to improve the paper.

References

1. M. Yamakawa, N. Nitta, T. Shiina, M. Matsumura, S. Tamano, T. Mitake, and E. Ueno, "High-speed freehand tissue elasticity imaging for breast diagnosis," Japanese J. Applied Physics 42, 3265-3270, 2003.
2. T. Shiina, M. Yamakawa, N. Nitta, E. Ueno, T. Matsumura, S. Tamano, and T. Mitake, "Clinical assessment of real-time freehand elasticity imaging system based on the combined autocorrelation method," Proc. IEEE Ultrason. Symp., 664-667, 2003.

3. T. Shiina, N. Nitta, E. Ueno, and J. C. Bamber, "Real time tissue elasticity imaging using the combined autocorrelation method," J. Med. Ultrason. 29, 119-128, 2002.
4. R. Y. Yoon, S. J. Kwon, M. H. Bae, and M. K. Jeong, "Improved ultrasonic elasticity imaging with center frequency estimation and global shift compensation," Proc. IEEE Ultrason. Symp., 1278-1281, 2006.
5. A. Pesavento, C. Perrey, M. Krueger, and H. Ermert, "A time-efficient and accurate strain estimation concept for ultrasonic elastography using iterative phase zero estimation," IEEE Trans. Ultrason. Ferroelect. Freq. Contr. 46, 1057-1067, 1999.
6. V. Shamdasani and Y. Kim, "Two-dimensional autocorrelation method for ultrasound-based strain estimation," Proc. IEEE Eng. Med. Biol., 1380-1383, 2004.
7. R. Zahiri-Azar and S. E. Salcudean, "Motion estimation in ultrasound images using time domain cross correlation with prior estimates," IEEE Trans. Biomed. Eng. 53, 1990-2000, 2006.
8. M. K. Jeong, S. J. Kwon, and D. G. Hyun, "An improved strain imaging method with a new image quality measure," Proc. Int'l Conf. Ultrason. Meas. Imag. Tissue Elasticity, 28, 2007.
9. J. Jiang, T. J. Hall, and A. M. Sommer, "A novel performance descriptor for ultrasonic strain imaging: A preliminary study," IEEE Trans. Ultrason. Ferroelect. Freq. Contr. 53, 1088-1102, 2006.
10. T. J. Hall, Y. Zhu, and C. S. Spalding, "In vivo real-time freehand palpation imaging," Ultrasound Med. Biol. 29, 427-435, 2003.
11. A. Pesavento, A. Lorenz, H. Ermert, H. Sommerfeld, M. Garcia-Schurmann, T. Senge, and S. Philippou, "Frame-to-frame statistics of real-time strain images," Proc. IEEE Ultrason. Symp., 1809-1812, 2000.
12. A. Pesavento, A. Lorenz, S. Siebers, and H. Ermert, "Frame to frame filtering of real time strain images," Proc. IEEE Ultrason. Symp. (abstract only), 2002.
13. T. Varghese and J. Ophir, "A theoretical framework for performance characterization of elastography: The strain filter," IEEE Trans. Ultrason. Ferroelect. Freq. Contr. 44, 164-172, 1997.
14. R. Kuc, "Generating a minimum-phase digital filter model for the acoustic attenuation of soft tissue," Proc. IEEE Ultrason. Symp., 794-796, 1983.
15. M. Bilgen and M. F. Insana, "Predicting target detectability in acoustic elastography," Proc. IEEE Ultrason. Symp., 1427-1430, 1997.
16. T. Varghese and J. Ophir, "An analysis of elastographic contrast-to-noise ratio," Ultrasound Med. Biol. 24, 915-924, 1998.
17. J. Ophir, I. Céspedes, H. Ponnekanti, Y. Yazdi, and X. Li, "Elastography: A quantitative method for imaging the elasticity of biological tissues," Ultrason. Imag. 13, 111-134, 1991.

[Profile]

• Mok-Kun Jeong

He received the B.S. degree in electrical engineering from Seoul National University in 1988, and the M.S. and Ph.D. degrees in electrical and electronic engineering from KAIST in 1990 and 1995, respectively. Presently, he is a professor in the Department of Electronics Engineering at Daejin University in Pocheon, Korea. His research interests are in the area of medical ultrasound signal processing.

•Sung-Jae Kwon

He received the B.S. degree in electronic engineering from Kyungpook National University in 1984, and the M.S. and Ph.D. degrees in electrical and electronic engineering from KAIST in 1986 and 1990, respectively. Presently, he is an associate professor in the Department of Communications Engineering at Daejin University in Pocheon, Korea. His research interests are in imaging, broadcasting, and communications systems.